Published in final edited form as:

Nat Methods. 2017 May ; 14(5): 479–482. doi:10.1038/nmeth.4257.

DeActs: genetically encoded tools for perturbing the actin cytoskeleton in single cells

Martin Harterink[1,7], **Marta Esteves da Silva**[1,7], **Lena Will**[1], **Julia Turan**[2], **Adiljan Ibrahim**[2], **Alexander E. Lang**[3], **Eljo Y. van Battum**[4], **R. Jeroen Pasterkamp**[4], **Lukas C. Kapitein**[1], **Dmitri Kudryashov**[5], **Ben A. Barres**[2], **Casper C. Hoogenraad**[1], and **J. Bradley Zuchero**[2,6]

[1]Cell Biology, Department of Biology, Faculty of Science, Utrecht University, Utrecht, The Netherlands [2]Department of Neurobiology, Stanford University School of Medicine, Stanford, California, USA [3]Institute for Experimental and Clinical Pharmacology and Toxicology, Albert-Ludwigs University of Freiburg, Freiburg, Germany [4]Department of Translational Neuroscience, Brain Center Rudolf Magnus, University Medical Center Utrecht, Utrecht, The Netherlands [5]Department of Chemistry and Biochemistry, The Ohio State University, Columbus, Ohio, USA [6]Department of Neurosurgery, Stanford University School of Medicine, Stanford, California, USA

Abstract

The actin cytoskeleton is essential for many fundamental biological processes, but tools to directly manipulate actin dynamics are limited to cell-permeable drugs precluding single cell perturbations. Here we describe DeActs, genetically encoded actin-modifying polypeptides, which effectively induce actin disassembly in eukaryotic cells. We demonstrate that DeActs are a universal tool for studying the actin cytoskeleton in single cells in culture, tissues, and multicellular organisms, including various neurodevelopmental model systems.

MAIN TEXT

Studying the role of the actin cytoskeleton is important for understanding many cell biological processes and the molecular basis of human diseases. Perturbation of the actin cytoskeleton is typically achieved using cell-permeable drugs, such as latrunculin or cytochalasin to promote actin disassembly[1,2]. However, these pharmacological approaches do not allow for cell-type specific perturbation, and therefore cannot be used to manipulate a subset of cells within complex multicellular model systems. Neuronal development is one example where the role of actin dynamics has been debated[3], in part due to the lack of

Correspondence should be addressed to: C.C.H. (c.c.hoogenraad@uu.nl) or J.B.Z. (zuchero@stanford.edu).
[7]These authors contributed equally to this work.

AUTHOR CONTRIBUTIONS

M.H., M.E.S., C.C.H., D.K., and J.B.Z. conceived the project. M.H., M.E.S., L.W., J.T., A.I., E.v.B., R.J.P., L.C.K., C.C.H., and J.B.Z. planned and/or executed experiments. A.E.L., D.K., and B.A.B. contributed essential reagents and expertise. M.H., M.E.S., C.C.H., and J.B.Z. wrote the paper with input from all authors. C.C.H. and J.B.Z. supervised all aspects of the work.

COMPETING FINANCIAL INTERESTS STATEMENT

The authors declare no competing financial interests.

proper tools to manipulate actin in single neurons in culture, tissues or multicellular organisms. The ideal tool to manipulate the actin cytoskeleton would (1) trigger disassembly of actin filaments, similar to latrunculin, (2) directly interact with actin, rather than inducing cytoskeletal changes indirectly through upstream signaling pathways, (3) be genetically encoded and not rely on the addition of ectopic cofactors[4], and (4) allow cellular visualization (e.g., as a GFP-fusion). Since actin is one of the most highly conserved proteins throughout eukaryotes this tool would also permit broad use in different experimental model systems.

To develop genetic tools that directly target the actin cytoskeleton (Disassembly-promoting, encodable Actin tools; DeActs), we screened both endogenous actin-binding domains that constitutively interact with actin and bacterial toxins that directly modify actin by transiently transfecting HeLa cells with candidate peptides (Fig. 1a and Supplementary Fig. 1). Gelsolin segment 1 (GS1) is a ~120 amino acid domain that sequesters actin monomers *in vitro* but lacks the severing activity and calcium-sensitivity of full-length gelsolin[5,6]. A GFP-GS1 (DeAct-GS1) fusion dramatically disrupted actin filaments when expressed in primary rat embryonic fibroblasts and HeLa cells, in contrast to GFP alone (Fig. 1b and Supplementary Fig. 1). Actin is a common target of pathogenic bacteria, and numerous species produce toxins that are specific to actin and either covalently modify it or bind directly[7]. *Salmonella enterica* SpvB is an ADP-ribosyltransferase that ADP-ribosylates actin monomers on a conserved arginine (Supplementary Fig. 2) to render them unable to polymerize[8], leading to net disassembly of all dynamic actin filaments. A GFP-fusion with the mono(ADP-ribosyl)transferase domain (DeAct-SpvB) caused complete loss of detectable actin filaments in cells (Fig. 1b). As expected, disrupting actin with both DeAct constructs caused defects in cellular actin filament levels and distribution (Fig. 1c–e), cell morphology, proliferation, and focal adhesions (Supplementary Fig. 3). Furthermore, live imaging revealed that DeActs caused profound defects in cell motility and loss of filopodia dynamics (Fig. 1f, Supplementary Fig. 3, and Supplementary Video 1). In all cases DeAct-SpvB caused more dramatic effects, which is consistent with DeAct-SpvB being an enzyme, while DeAct-GS1 binds stoichiometrically to actin[5] and thus requires higher expression to induce actin disassembly. Consistently, cell motility was only inhibited at high expression of DeAct-GS1 (Fig. 1f and Supplementary Video 2), whereas low levels of DeAct-SpvB expression were sufficient to cause efficient actin disassembly (Fig. 1d) and inhibit cell motility (Fig. 1f and Supplementary Fig. 3). To look more closely at the dose-dependence of DeAct-GS1, we made use of the observation that differentiated oligodendrocyte cells (OLs) do not require an intact actin cytoskeleton to maintain a flattened cell morphology[9]. Expressing DeAct-GS1 under control of a mature OL promoter[10] induced a dose-dependent loss of actin filaments without causing cell retraction (Fig 1g and Supplementary Fig. 3). Finally, to allow inducible DeAct expression we made use of the TetOn-3G system (Clontech), which resulted in rapid DeAct expression, efficient actin disruption, and inhibition of cell motility following addition of doxycycline (Supplementary Fig. 4). By adding a constitutively expressed mCherry to the opposite DNA strand, we also allowed visualization of transfected cells prior to induction of DeAct expression (Supplementary Fig. 5). To suppress background expression of SpvB in the absence of doxycycline, we fused a DHFRdd destabilization domain[11] to SpvB to attenuate its expression (Supplementary Fig. 5). Together, these DeAct

constructs represent a toolkit for rapid and tunable perturbation of the actin cytoskeleton in cells and their simultaneous visualization.

We next tested whether DeActs could be used to study the role of actin dynamics in other cellular model systems, such as developing neurons in culture. Primary hippocampal neurons expressing DeAct-GS1 and DeAct-SpvB revealed a robust cell-specific decrease in actin filaments in the axonal growth cone, highly similar to latrunculin-treated neurons (Fig. 2a–c). Growth cone morphology was severely altered with DeAct expression or after latrunculin treatment, with a marked shift from fan- or torpedo-like shape (exploratory and elongating growth cones) to bulb and collapsed shape (stationary or eliminating growth cones)[12] (Fig. 2a,d). Whereas in control conditions more than 40% of axonal tips were dynamic, subsequent treatment with latrunculin markedly decreased dynamics as expected (Fig. 2e,f and Supplementary Video 3). Consistently, DeAct expression inhibited axonal growth cone dynamics to a similar extent as latrunculin (Fig. 2e and Supplementary Video 3). Thus, DeActs disrupt the actin cytoskeleton in a cell-specific manner and cause neuronal morphology defects.

A major advantage of genetically encoded DeActs is the ability to use them in multicellular organisms where cytoskeletal drugs may have broader effects and/or are more difficult to administer. The first *in vivo* system we used was the developing embryonic mouse neocortex, where newly born neurons polarize and migrate from the ventricular zone towards the cortical plate[13]. We electroporated DeAct DNA constructs into the brains (motor cortices) of E14.5 mouse embryos *in utero* and allowed them to develop for 3 days prior to sacrificing and analyzing cortical migration. In control animals, GFP-positive neurons migrated efficiently to the upper layers of the cortical plate (Fig. 2g–i). In contrast, expression of DeAct-GS1 led to a marked decrease in the number of neurons that reached the upper cortical layers (Fig. 2i), although no clear morphological differences were observed (Fig. 2j,k), Consistent with our culture studies, neurons expressing DeAct-SpvB failed to become bipolar and did not migrate towards the cortical plate, but instead accumulated in the subventricular zone (Fig 2g–i). Thus, DeActs cause strong developmental defects during neuronal migration *in vivo*.

As a second *in vivo* model we used the nematode *C. elegans*, for which conventional drugs are hard to use due to its impermeable exoskeleton. The PVD sensory neuron possesses a stereotyped morphology with two highly branched dendrites (anterior and posterior) and an axon that extends first ventrally and then anteriorly into the ventral nerve cord (Fig. 3a). We first found that the moesin-based actin marker moeABD[14] was enriched in the many dendritic side branches (Fig. 3b). We expressed DeActs using a specific PVD neuron promoter that is activated early during neurite extension[15]. Consistent with a role for actin assembly, PVD neuron-specific DeAct expression led to severe loss of dendrite branching (Fig. 3b–d). In addition to branching, primary neurite outgrowth was largely blocked upon DeAct-SpvB expression or high expression of DeAct-GS1 (Fig. 3e–g). Thus, DeAct-SpvB led to strong neuronal phenotypes *in vivo* whereas the severity of the DeAct-GS1 induced phenotypes was dose-dependent.

In conclusion, by repurposing the actin binding domain of gelsolin (DeAct-GS1) and the actin-modifying enzymatic activity of SpvB (DeAct-SpvB), we created novel tools that allow for cell-specific perturbation of the actin cytoskeleton both in cultured cells and multicellular *in vivo* model systems. Having genetically encoded tools allows for control of actin dynamics using cell type-specific and inducible promoters, and opens up new possibilities for elucidating the role of actin dynamics in fundamental and disease relevant cellular processes.

DATA AVAILABILITY

The data that support the findings of this study and detailed protocols for all methods are available from the corresponding authors upon request. The following plasmids have been deposited at Addgene: pCMV-DeAct-GS1 (Addgene plasmid 89445), pCMV-DeAct-SpvB (Addgene plasmid 89446), pTetON-EGFP (Addgene plasmid 89453), pTetON-DeAct-GS1 (Addgene plasmid 89454), and pTetON-DHFRdd-SpvB; CMV-mCherry (Addgene plasmid 89463). Other plasmids are available upon request.

ONLINE METHODS

Ethics Statement

All animal experiments were performed in compliance with the guidelines for the welfare of experimental animals issued by the Government of The Netherlands. All animal experiments were approved by the Animal Ethical Review Committee (DEC) of Utrecht University or were approved by Stanford University's Administrative Panel on Laboratory Animal Care.

Molecular biology and design of DeActs

We used published biochemical data to determine the minimal actin binding or modifying domains of Gelsolin (Gelsolin segment 1, GS1)[5,6,16,17], *Salmonella enterica* SpvB (mono(ADP-ribosyl)transferase domain)[8,18,19], *Vibrio cholerae* $MARTX_{VC}$ (actin crosslinking domain)[20,21], *Salmonella* SipA (actin crosslinking minimal domain)[22], *Photorhabdus luminescens* TccC3 (mono(ADP-ribosyl)transferase domain)[23], and *Clostridium botulinum* C2I (mono(ADP-ribosyl)transferase domain)[24,25]. Despite extensive biochemical data on the mechanisms, specificity, and minimal functional domains of these peptides[5–8,16–19] they have not previously been developed as cell biological tools. DNA sequences encoding candidate peptides were cloned into pEGFP-C1 (Clontech) by standard procedures. To create constitutively active cofilin (GFP-P2A-cofilin(S3A)[26]) we first inserted DNA encoding a P2A self-cleavable peptide into the multicloning site of pEGFP-C1, then inserted DNA encoding full-length human cofilin(S3A) (kind gift of Brittany Belin) in frame on the C-terminal side. In the case of DeAct-GS1 and DeAct-SpvB we truncated proteins within regions predicted to be disordered[27].

The following mammalian expression plasmid have been described previously: tagRFP-paxillin[28], pGW2-MARCKS-eGFP[29], pSuper vector[30], pβactin-GFP[31], *E. coli* dihydrofolate reductase destabilization domain (DHFRdd) with R12Y, G67S, Y100I mutations[11] was a gift of Tom Wandless and Ling-chun Chen. pGW2-MARCKS-TagRFP-T was generated by introducing Tag-RFP-T to GW2-MARCKS by PCR strategy. For the *in utero* experiments,

DNA encoding DeAct-GS1 and DeAct-SpvB were cloned into the pGW2-GFP vector. For the *C. elegans* experiments the *Pdes-2::mKate2::GS1* and *Pdes-2::mKate2::SpvB* were cloned using multisite Gateway cloning. The *des-2* promoter sequence was based on Maniar et al (2012)[15] and cloned into pDONR4-1, the mKate2 sequence (kind gift from Henrik Bringmann[32]) was cloned into pDONR221 and the DeAct-GS1 or DeAct-SpvB sequences were cloned into pDONR2–3. pKN146 was used as destination vector which is the pCFJ201 vector supplemented with the *unc-54* UTR (kind gift from H.C. Korswagen). The cytoplasmic mKate2 was cloned into the pCFJ150[33] using the pCM1.36 *tbb-2* UTR (Addgene #17249). All constructs were validated by sequencing. Gelsolin and SpvB sequences used for in DeAct constructs are as follows.

DeAct-GS1 (human *GSN*; Genbank NM_000177.4; sequence encoding amino acids #53-176)

GTGGTGGAACACCCCGAGTTCCTCAAGGCAGGGAAGGAGCCTGGCCTGCAGATC
TGGCGTGTGGAGAAGTTCGATCTGGTGCCCGTGCCCACCAACCTTTATGGAGACT
TCTTCACGGGCGACGCCTACGTCATCCTGAAGACAGTGCAGCTGAGGAACGGAA
ATCTGCAGTATGACCTCCACTACTGGCTGGGCAATGAGTGCAGCCAGGATGAGAG
CGGGGCGGCCGCCATCTTTACCGTGCAGCTGGATGACTACCTGAACGGCCGGGCC
GTGCAGCACCGTGAGGTCCAGGGCTTCGAGTCGGCCACCTTCCTAGGCTACTTCA
AGTCTGGCCTGAAGTACAAGAAAGGAGGTGTGGCATCAGGATTC

DeAct-SpvB (*Salmonella enterica spvB*; Genbank D14490.1; sequence encoding amino acids #375-591)

GGAGGTAATTCATCTCGACCAAAATCAAAATGGGCGATTGTAGAGGCATCAAAGC
AGATTCAAGCTCTGAGGTACTATTCAGCTCAAGGGTACAGTGTGATTAATAAATATT
TACGTGGGGATGATTATCCTGAAACACAGGCAAAAGAAACTCTGCTCTCCAGAGA
CTATCTTTCCACAAATGAACCCAGTGATGAGGAGTTTAAAAATGCCATGTCAGTTT
ATATAAATGATATTGCGGAGGGATTAAGTTCACTTCCCGAAACAGATCACAGAGTC
GTATACCGGGGCCTGAAGCTTGATAAGCCCGCATTATCGGATGTGCTGAAGGAATA
CACTACTATAGGTAATATAATAATAGATAAAGCTTTTATGAGTACATCGCCAGATAAG
GCATGGATAAATGACACTATTCTCAACATATACCTAGAAAAAGGACATAAAGGTAG
AATACTCGGAGATGTTGCACATTTTAAGGGAGAGGCAGAGATGCTTTTCCCTCCA
AATACTAAACTCAAAATCGAAAGCATTGTAAATTGTGGATCCCAAGACTTTGCAA
GCCAGCTTAGTAAGCTGAGATTAAGTGATGATGCAACTGCTGACACAAACAGGAT
AAAAAGAATAATAAACATGAGGGTACTCAACTCA

Cell culture experiments

HeLa cells (American Type Culture Collection) were cultured in DMEM medium (Life Technologies) supplemented with 10% FBS, 2 mM L-glutamine, nonessential amino acids, and penicillin/streptomycin (all from Gibco) at 37°C with 5% CO_2. We used cells from ATCC for <5 passages so did not authenticate or test for mycoplasma contamination in-house. HeLa Tet-On 3G stable cell line (Clontech #631186) were cultured in the same media, but with Tet System Approved FCS that is guaranteed to have no contaminating tet/dox (Clontech). Expression from the TetON promoter was induced with doxycycline (1–100 ng/mL as noted; Sigma D9891). Primary rat embryonic fibroblasts (REFs) were isolated

as previously described[34] and plated in the same growth media. For transfection, cells were seeded onto glass coverslips one day prior and transfected using XtremeGENE HP DNA Transfection Reagent (Roche) or Fugene (Roche) according to the manufacturer's protocol, or treated with latrunculin A (EMD Millipore) to induce actin disassembly. OPCs were purified from enzymatically dissociated, mixed-sex P7-P8 Sprague-Dawley (Charles Rivers) rat brains by immunopanning and grown in serum-free defined medium, as described previously[35]. PDGF (10 ng/ml, PeproTech) and NT-3 (1 ng/ml, PeproTech) were added to the media to induce OPC proliferation. OPCs were transfected as described previously[35] using a Lonza/Amaxa nucleofector kit, with 2–3 x 10^6 OPCs per transfection, then differentiated into mature OLs by removal of PDGF and NT-3 and addition of thyroid hormone (triiodothyronine, T3; 40 ng/ml; Sigma) as described[35]. We used the myelin basic protein promoter (MBPp)[10] for expression of DeActs in mature OLs.

Cells were fixed in 4% formaldehyde (prepared from paraformaldehyde) for 15 min, permeabilized with 0.1% Triton X-100 for 3 min, then blocked in 3% BSA in PBS. Native GFP fluorescence was visualized to detect DeAct expression. Cells were stained with Alexa Fluor 594-phalloidin (Invitrogen) to visualize actin filaments, DAPI to visualize nuclei, HCS CellMask Blue (Invitrogen) to reveal cellular morphology, or immunostained for myelin basic protein (MBP) to detect oligodendrocytes (Abcam ab7349, used at 1:100). Cells were visualized by epifluorescence using a Zeiss Axio Imager M1 and Axiovision software, most frequently with a 20x 0.8 NA Plan Apo objective, or by confocal using an LSM510 scan head on an Axio Observer Z1 with either a 63x 1.4 NA objective (all of the above, Carl Zeiss Microscopy). Identical illumination and acquisition conditions were used for each experiment. Confocal images of HeLa cells for focal adhesion quantification were acquired using LSM700 (Zeiss) with a 40x/1.30 Oil DIC objective using 488nm and 555nm laser lines. A total thickness of 5 μm was scanned for each position and maximum intensity projections were generated for analysis.

Hippocampal neuron cultures, transfections and drug treatments

Primary hippocampal cultures were prepared from mixed sex embryonic day 18 (E18) Wistar rat brains[36,37]. Cells were plated on coverslips coated with poly-L-lysine (37.5 μg/ml) and laminin (1.25 μg/ml) at a density of 100,000/well. Hippocampal cultures were grown in Neurobasal medium (NB) supplemented with B27, 0.5 mM glutamine, 15.6 μM glutamate and penicillin/streptomycin. Hippocampal neurons at DIV2 were transfected using Lipofectamine 2000 (Invitrogen). Briefly, DNA (3.6 μg /well) was mixed with 3 μl Lipofectamine 2000 in 200 μl NB, incubated for 30 minutes and then added to the neurons in NB with 0.5mM glutamine at 37°C in 5% CO_2 for 45 min to 1 hour. Next, neurons were washed with NB and transferred in the original medium at 37°C in 5% CO_2 for 36–48 hours. Neurons were co-transfected with GFP-tagged MARCKS (control), GS1 or SpvB together with empty pSuper vector. Whenever indicated 10 μM latrunculin B (Sigma) was added to the neuron cultures and either imaged 1 min and up to 30minutes after addition or fixed after 30 minutes.

Neuron immunocytochemistry, growth cone morphology and phalloidin intensity analysis

For immunocytochemistry, neurons were fixed for 10 min with 4% formaldehyde/4% sucrose in PBS at room temperature. After fixation cells were washed 3 times for 5 minutes in PBS at room temperature and incubated with Alexa Fluor 568-phalloidin (Life Technologies A12380) for 1 hour at room temperature. Neurons were then washed 3 times for 5 minutes in PBS at room temperature and subsequently mounted on slides in Vectashield mounting medium (Vector Laboratories). Confocal images were acquired using LSM700 (Zeiss) with a 63x/1.40 Oil or 40x/1.30 Oil DIC objective using 488nm and 555nm laser lines. A total thickness of 5 μm was scanned for each position and maximum intensity projections were generated for analysis. Imaging settings were kept the same when pictures were compared for fluorescence intensity. Growth cone morphology was classified manually and phalloidin intensity was measured in ImageJ. The entire growth cone areas were considered and normalized to growth cones of untransfected neighboring neurons.

To be able to identify the axon in the live cell imaging experiments, neuronal cultures were incubated with extracellular Neurofascin-pan mouse primary antibody (NeuroMab, clone number A12/18) in conditioned Neurobasal medium, for 10 minutes at 37°C. After this, neurons were washed 3 times in warm Neurobasal medium and anti-mouse Alexa405 antibody (Life Technologies, catalogue number A31553) in conditioned Neurobasal medium was added for 10 minutes at 37°C. Neurons were then washed 3 times in warm Neurobasal medium and returned to the conditioned medium.

Live cell imaging microscopy

All imaging was performed in full conditioned medium at 37°C and 5% CO_2 unless otherwise indicated. For live imaging of REF cell motility, cells were plated on PDL-coated plastic bottom ImageLock plates (Essen Bioscience) and imaged in an IncuCyte ZOOM Live Cell Imaging System (Essen Bioscience) with 10% CO_2. For wound healing assays, cells were plated on 5 μg/mL fibronectin, grown until confluent, then mechanically scratch-wounded with a sterile p2 pipette tip. Non-adhered cells were washed off with fresh growth media and imaged once per hour. Live cell imaging of hippocampal neurons was performed by laser confocal spinning disk microscopy, using a Nikon Eclipse-Ti (Nikon) microscope with Plan Apo 40x N.A. 1.30 oil objective (Nikon. The microscope is equipped with a motorized stage (ASI; MS-2000), a Perfect Focus System (Nikon), an incubation chamber (Tokai Hit; INUBG2E-ZILCS) and uses MetaMorph 7.7.6 software (Molecular Devices) to control the camera and all motorized parts. Confocal excitation and detection is achieved using 100 mW Cobolt Calypso 491nm and 100mW Cobolt Jive 561nm lasers and a Yokogawa spinning disk confocal scanning unit (CSU-X1-A1; Yokogawa) equipped with a triple-band dichroic mirror (z405/488/568trans-pc; Chroma) and a filter wheel (CSU-X1-FW-06P-01; Yokogawa) containing BFP (ET-BFP 49021), GFP (ET-GFP (49002)), mCherry (ET-mCherry (49008)) and mCherry/GFP (ET-mCherry/GFP (59022)) emission filters (all Chroma). Confocal images were acquired with a Evolve 512 EMCCD camera (Photometrics) at a final magnification of 67 nm/pixel, including the additional 2.0× magnification introduced by an additional lens mounted between scanning unit and camera (Edmund Optics). For quantifying single cell motility of fibroblasts, we first imaged the GFP channel to identify GFP- or DeAct-expressing cells, then subsequently imaged with phase

microscopy to limit phototoxicity until the final frame of the movie, with 15 minute intervals. To classify DeAct-GS1 expressing cells as high or low expressers, we quantified average cellular GFP intensity from initial fluorescence images (background subtracted, ImageJ), and defined high expressers as those cells with GFP signals above the median value. Cell motility was measured in ImageJ by first aligning images with the StackReg plugin, then measuring displacement of the nucleus using the MTrackJ plugin.

Axonal branches were imaged in time lapses of 5 minutes, with 5 seconds interval between acquisition and a z-stack stream at every time point, to guarantee the entire axonal branch complexity is imaged. In control conditions (MARCKS-eGFP), 5–6 neurons were first imaged in Neurobasal medium. After that 10 μM latrunculin B (Sigma) was added to the imaging chamber and the same cells were imaged from 1 to 30 minutes. The dynamics of axonal branches was quantified manually using ImageJ.

Time-lapse live-cell imaging of filopodia dynamics in HeLa cells was performed using a TIRF microscope (Nikon Eclipse TE2000E) equipped with an incubation chamber (Tokai Hit; INUG2-ZILCS-H2) mounted on a motorized stage (Prior). Cells were imaged in full medium at 37°C and 5% CO2 every 5 seconds for 5 minutes using a 100x objective (Apo TIRF 100x/NA 1.49, Nikon) and an Evolve 512 EMCCD camera (Photometrics)[38]. Excitation was achieved using a 488 nm LuxX488-100 diode laser and a 561 nm Cobolt Jive laser, fiber-coupled to the Nikon TIRF module. GFP-expressing cells treated with Latrunculin B were first imaged without the drug and then imaged again after 5 to 30 minutes upon addition of 10 μM of Latrunculin. Quantification of total and dynamic filopodia numbers was performed using ImageJ.

In utero electroporation and immunohistochemistry

Pregnant C57Bl/6 mice at E14.5 were deeply anaesthetized with Isofluorane (induction: 3–4%, surgery, 1.5–2%), injected with 0.05mg/kg buprenorfinhydrocloride in saline, and hereafter the abdominal cavity was opened under sterile surgical conditions. Uterine horns were exposed and 1.7ul DNA mixture containing (pGW2-GFP alone or together with DeAct-GS1 or DeAct-SpvB) dissolved in MilliQ water with 0.05% Fast Green (Sigma) was injected in the lateral ventricles of the embryo's using glass micropipettes (Harvard Apparatus) and a PLI-200 Pico-injector (Harvard Apparatus). Brains (motor cortex) were electroporated with gold plated tweezer-electrodes (Fischer Scientific) using and ECM 830 Electro-Square-Porator (Harvard Apparatus) set to three unipolar pulses at 30V (100ms interval and pulse length). Embryos were placed back into the abdomen, and abdominal muscles and skin were sutured separately. The mother mice were awakened by releasing them from Isofluorane. Embryos were collected at E17.5 and brains were fixed in 4% formaldehyde and submerged in 30% sucrose. 12μm coronal brain cryosections were made and were blocked and permeabilized in 10% Normal Horse Serum + 0.2% Triton X-100 in PBS prior to staining with first antibody (anti-GFP, MBL-Sanbio; anti-Ctip2, Abcam; anti-Neurofilament heavy chain, Abcam; and anti-Satb2, Abcam) in blocking solution overnight and fluorescent secondary antibody staining (Alexa 488, Alexa 568 and Alexa 647, Life technologies) and mounting with Vectashield mounting medium (Vectorlabs). Confocal images were acquired using LSM700 (Zeiss) with a 20x/ 0.8 objective using 405nm, 488nm,

555nm and 633nm laser lines. A total thickness of 15 μm in 1 μm steps was scanned for each position and maximum intensity projections were generated for analysis. To cover the entire brain slice, 4 images were taken side-by-side and image stitching was performed using ZEN 2011 Software.

C. elegans strains, transgenes and imaging

Strains were cultured using standard conditions[39] at 15 °C and imaged at room temperature at the L4 or young adult stage. For the PVD morphology experiments the DeAct-GS1 and DeAct-SpvB constructs were injected in either NC1686 (*wdIs51*), which expressed GFP in the PVD, or in STR58 (*hrtIs3[Pdes-2::myristoylGFP;unc-122::DsRed]*), which is an integrant of CX11480 (*kyEx3017*)[15], generating: STR198 *hrtIs3;hrtEx52[Pdes-2::mKate2::GS1(20ng/μl);Pmyo-2::tdTom]*, STR199 *wdIs51;hrtEx53[Pdes-2::mKate2::GS1(4ng/μl);Pmyo-2::tdTom]*, STR200 *hrtIs3;hrtEx54[Pdes-2::mKate2::SpvB(4ng/μl);Pmyo-2::tdTom]*. The Actin marker strains were generated using a construct expressing the moesin actin binding domain (kind gift from Kang Shen[14]), generating: STR213 *hrtEx60[Punc-86::GFP::moeABD;Pdes-2::mKate2;Pmyo-2::tdTom]*, STR232 *hrtEx68[Pdes-2::mKate2::GS1(20ng/μl);Punc-86::GFP::moeABD;Pmyo-2::tdTom]*. Worms were anesthetized with 10 mM tetramisole, imaged by confocal microscopy and maximum intensity projections of acquired Z stacks (1 μm steps) and straightening of the animal was done using ImageJ software (Universal Imaging Corporation).

Data analysis and statistics

All data acquisition and analysis were performed blinded to the experimental condition. We used nested analysis to first average technical replicates (e.g., three coverslips). In all cases *N* refers to number of independent experiments for cell culture experiments, or number of mice or worms for in vivo experiments (while *n* refers to technical replicates). Sample sizes used were similar to those generally employed in the field. Animals were allocated randomly to each experimental group. Data shown are from all animals tested; none were treated as outliers. Micrographs were analyzed using NIH ImageJ and linearly contrast adjusted for display using Adobe Photoshop, with identical settings for each experiment. For quantification of fluorescent and phase micrographs, ROIs were drawn by hand or by thresholding multichannel images using ImageJ (NIH). Mean gray value (average intensity) of each individual channel was measured, and background (outside of cell area) was subtracted for each micrograph. Qualitative scoring of abnormal actin in cells was performed by an investigator blinded to experimental condition. In our hands untransfected rat embryonic fibroblasts had stereotyped phalloidin staining with similar filament intensities and distribution (e.g. stress fibers and cortical actin). GFP+ cells were considered abnormal if they had dim phalloidin staining or disorganized actin filaments (lacking stress fibers and/or presence of actin filament foci as in latrunculin-treated cells), excluding mitotic cells. Data were analyzed and plotted using Excel (Microsoft) and Prism (GraphPad Software). Unless otherwise stated, error bars are SEM, and p values were calculated using Student's t test for single comparisons or ANOVA followed by Dunnett's multiple comparison test, assuming equal variance.

Supplementary Material

Refer to Web version on PubMed Central for supplementary material.

Acknowledgments

We thank C. Bargmann (Rockefeller) for the CX11480 strain, K. Shen (Stanford) for the moesin actin marker, K. Satchell (Northwestern) for MARTX$_{VC}$, K. Aktories (Albert-Ludwigs University of Freiburg) for TccC3 and C2I, D. Mullins (UCSF) for cofilin(S3A), T. Wandless (Stanford) for DHFRdd; L.-c. Chen, L. Spector, E. Vitriol, and M.Z. Lin for reagents and helpful discussions; Wormbase; and Stanford Neuroscience Microscopy Service, supported by NIH NS069375. We gratefully acknowledge funding from the Netherlands Organization for Scientific Research (NWO) (NWO-ALW-VENI to M.H., NWO-ALW-VICI to C.C.H., NWO-ALW-VICI to R.J.P., the European Research Council (ERC Consolidator Grant; C.C.H.), the Deutsche Forschungsgemeinschaft (Germany) project AK6/22-2 (A.E.L.), NIH R01 GM114666 (D.K.), the National Multiple Sclerosis Society (J.B.Z and B.A.B), NIH R01 EY10257 (B.A.B.), and the Dr. Miriam and Sheldon G. Adelson Medical Research Foundation (B.A.B). M.E.d.S. is supported by Fundação para a Ciência e Tecnologia (FCT, Portugal; grant SFRH/BD/68642/2010). J.B.Z. is a Career Transition Award Fellow of the National Multiple Sclerosis Society.

References

1. Spector I, Shochet NR, Kashman Y, Groweiss A. Latrunculins: novel marine toxins that disrupt microfilament organization in cultured cells. Science. 1983; 219:493–495. [PubMed: 6681676]
2. MacLean-Fletcher S, Pollard TD. Mechanism of action of cytochalasin B on actin. Cell. 1980; 20:329–341. [PubMed: 6893016]
3. Vitriol EA, Zheng JQ. Growth cone travel in space and time: the cellular ensemble of cytoskeleton, adhesion, and membrane. Neuron. 2012; 73:1068–1081. [PubMed: 22445336]
4. Wu YI, et al. A genetically encoded photoactivatable Rac controls the motility of living cells. Nature. 2009; 461:104–108. [PubMed: 19693014]
5. Way M, Pope B, Gooch J, Hawkins M, Weeds AG. Identification of a region in segment 1 of gelsolin critical for actin binding. EMBO J. 1990; 9:4103–4109. [PubMed: 2174356]
6. McLaughlin PJ, Gooch JT, Mannherz HG, Weeds AG. Structure of gelsolin segment 1-actin complex and the mechanism of filament severing. Nature. 1993; 364:685–692. [PubMed: 8395021]
7. Aktories K, Lang AE, Schwan C, Mannherz HG. Actin as target for modification by bacterial protein toxins. FEBS Journal. 2011; 278:4526–4543. [PubMed: 21466657]
8. Margarit SM, Davidson W, Frego L, Stebbins CE. A steric antagonism of actin polymerization by a salmonella virulence protein. Structure. 2006; 14:1219–1229. [PubMed: 16905096]
9. Zuchero JB, et al. CNS myelin wrapping is driven by actin disassembly. Dev Cell. 2015; 34:152–167. [PubMed: 26166300]
10. Gow A, Friedrich VL, Lazzarini RA. Myelin basic protein gene contains separate enhancers for oligodendrocyte and Schwann cell expression. J Cell Biol. 1992; 119:605–616. [PubMed: 1383235]
11. Iwamoto M, Björklund T, Lundberg C, Kirik D, Wandless TJ. A general chemical method to regulate protein stability in the mammalian central nervous system. Chem Biol. 2010; 17:981–988. [PubMed: 20851347]
12. van der Vaart B, et al. CFEOM1-associated kinesin KIF21A is a cortical microtubule growth inhibitor. Dev Cell. 2013; 27:145–160. [PubMed: 24120883]
13. Barnes AP, Polleux F. Establishment of axon-dendrite polarity in developing neurons. Annu Rev Neurosci. 2009; 32:347–381. [PubMed: 19400726]
14. Chia PH, Patel MR, Shen K. NAB-1 instructs synapse assembly by linking adhesion molecules and F-actin to active zone proteins. Nat Neurosci. 2012; 15:234–242. [PubMed: 22231427]
15. Maniar TA, et al. UNC-33 (CRMP) and ankyrin organize microtubules and localize kinesin to polarize axon-dendrite sorting. Nat Neurosci. 2012; 15:48–56.
16. Way M, Pope B, Weeds AG. Are the conserved sequences in segment 1 of gelsolin important for binding actin? J Cell Biol. 1992; 116:1135–1143. [PubMed: 1310993]

17. Finidori J, Friederich E, Kwiatkowski DJ, Louvard D. In vivo analysis of functional domains from villin and gelsolin. J Cell Biol. 1992; 116:1145–1155. [PubMed: 1310994]
18. Tezcan-Merdol D, et al. Actin is ADP-ribosylated by the Salmonella enterica virulence-associated protein SpvB. Mol Microbiol. 2001; 39:606–619. [PubMed: 11169102]
19. Hochmann H, Pust S, von Figura G, Aktories K, Barth H. Salmonella enterica SpvB ADP-Ribosylates Actin at Position Arginine-177. Characterization of the Catalytic Domain within the SpvB Protein and a Comparison to Binary Clostridial Actin-ADP-Ribosylating Toxins. Biochemistry. 2006; 45:1271–1277. [PubMed: 16430223]
20. Sheahan KL, Cordero CL, Satchell KJF. Identification of a domain within the multifunctional Vibrio cholerae RTX toxin that covalently cross-links actin. Proc Natl Acad Sci USA. 2004; 101:9798–9803. [PubMed: 15199181]
21. Kudryashov DS, et al. Connecting actin monomers by iso-peptide bond is a toxicity mechanism of the Vibrio cholerae MARTX toxin. Proc Natl Acad Sci USA. 2008; 105:18537–18542. [PubMed: 19015515]
22. Lilic M, et al. Salmonella SipA polymerizes actin by stapling filaments with nonglobular protein arms. Science. 2003; 301:1918–1921. [PubMed: 14512630]
23. Lang AE, et al. Photorhabdus luminescens toxins ADP-ribosylate actin and RhoA to force actin clustering. Science. 2010; 327:1139–1142. [PubMed: 20185726]
24. Vandekerckhove J, Schering B, Bärmann M, Aktories K. Botulinum C2 toxin ADP-ribosylates cytoplasmic beta/gamma-actin in arginine 177. J Biol Chem. 1988; 263:696–700. [PubMed: 3335520]
25. Schleberger C, Hochmann H, Barth H, Aktories K, Schulz GE. Structure and action of the binary C2 toxin from Clostridium botulinum. J Mol Biol. 2006; 364:705–715. [PubMed: 17027031]
26. Agnew BJ, Minamide LS, Bamburg JR. Reactivation of phosphorylated actin depolymerizing factor and identification of the regulatory site. J Biol Chem. 1995; 270:17582–17587. [PubMed: 7615564]
27. Li X, Romero P, Rani M, Dunker A, Obradovic Z. Predicting Protein Disorder for N-, C-, and Internal Regions. Genome Inform Ser Workshop Genome Inform. 1999; 10:30–40.
28. Bouchet BP, et al. Talin-KANK1 interaction controls the recruitment of cortical microtubule stabilizing complexes to focal adhesions. eLife. 2016; 5
29. Schätzle P, et al. Rapid and reversible formation of spine head filopodia in response to muscarinic receptor activation in CA1 pyramidal cells. J Physiol (Lond). 2011; 589:4353–4364. [PubMed: 21768266]
30. Brummelkamp TR, Bernards R, Agami R. A system for stable expression of short interfering RNAs in mammalian cells. Science. 2002; 296:550–553. [PubMed: 11910072]
31. Kapitein, et al. Probing intracellular motor protein activity using an inducible cargo trafficking assay. Biophys J. 2010; 99:2143–52. [PubMed: 20923648]
32. Redemann S, et al. Codon adaptation-based control of protein expression in C. elegans. Nat Meth. 2011; 8:250–252.
33. Frøkjaer-Jensen C, et al. Single-copy insertion of transgenes in Caenorhabditis elegans. Nat Genet. 2008; 40:1375–1383. [PubMed: 18953339]
34. Vierbuchen T, et al. Direct conversion of fibroblasts to functional neurons by defined factors. Nature. 2010; 463:1035–1041. [PubMed: 20107439]
35. Dugas JC, Tai YC, Speed TP, Ngai J, Barres BA. Functional genomic analysis of oligodendrocyte differentiation. J Neurosci. 2006; 26:10967–10983. [PubMed: 17065439]
36. Goslin K, Banker G. Experimental observations on the development of polarity by hippocampal neurons in culture. J Cell Biol. 1989; 108:1507–1516. [PubMed: 2925793]
37. Kapitein LC, Yau KW, Hoogenraad CC. Microtubule dynamics in dendritic spines. Methods Cell Biol. 2010; 97:111–132. [PubMed: 20719268]
38. Kapitein, et al. Myosin-V opposes microtubule-based cargo transport and drives directional motility on cortical actin. Curr Biology. 2013; 23:828–834.
39. Brenner S. The genetics of Caenorhabditis elegans. Genetics. 1974; 77:71–94. [PubMed: 4366476]

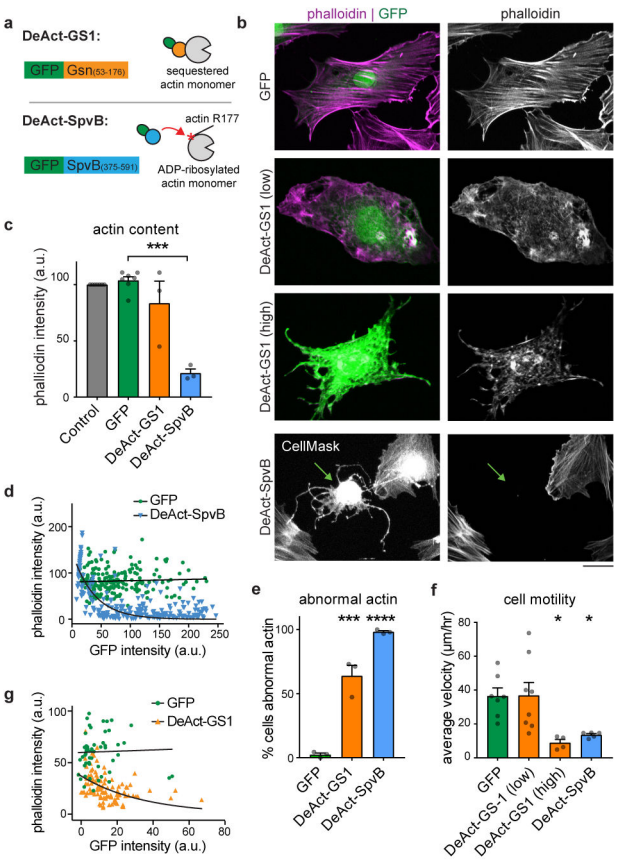

Figure 1. Construction and characterization of DeActs

(**a**) Schematic of DeAct constructs and mechanism of action.

(**b**) Expression of DeActs in rat embryonic fibroblasts, visualized with GFP and Alexa Fluor 594-phalloidin. CellMask Blue was used to reveal full cell morphology upon DeAct-SpvB expression. Scale, 20 μm. Representative micrographs from $N = 4$ independent experiments.

(**c–e**) Quantification of DeAct effect on actin in rat embryonic fibroblasts showing (**c**) average phalloidin intensities ($N = 7, 7, 3, 3$ independent experiments, left to right), (**d**) phalloidin intensity relative to the DeAct-SpvB level ($n = 207$ GFP or 240 DeAct-SpvB cells), and (**e**) percent of cells with abnormal actin filament distribution ($N = 3$ independent experiments; see Supplementary Methods).

(**f**) Velocities of single cell motility of rat embryonic fibroblasts transfected with DeActs or GFP control (see also Supplementary Video 2). $n = 7, 8, 4$, or 5 expressing cells per condition, left to right.

(**g**) Oligodendrocyte-specific expression of GFP or DeAct-GS1 in primary rat oligodendrocytes using the OL-specific myelin basic protein promoter, quantifying phalloidin intensity relative to the DeAct-GS1 level (fluorescence intensities not directly comparable to panel **d**). $n = 55$ GFP or 103 DeAct-GS1 cells.

Graphs show mean ± SEM. Trend lines in **d** and **g** show nonlinear (exponential) fit; each data point is one cell. Statistical significance: one-way ANOVA followed by Dunnett's multiple comparison test, ****p<0.0001, ***p<0.001, *p<0.05.

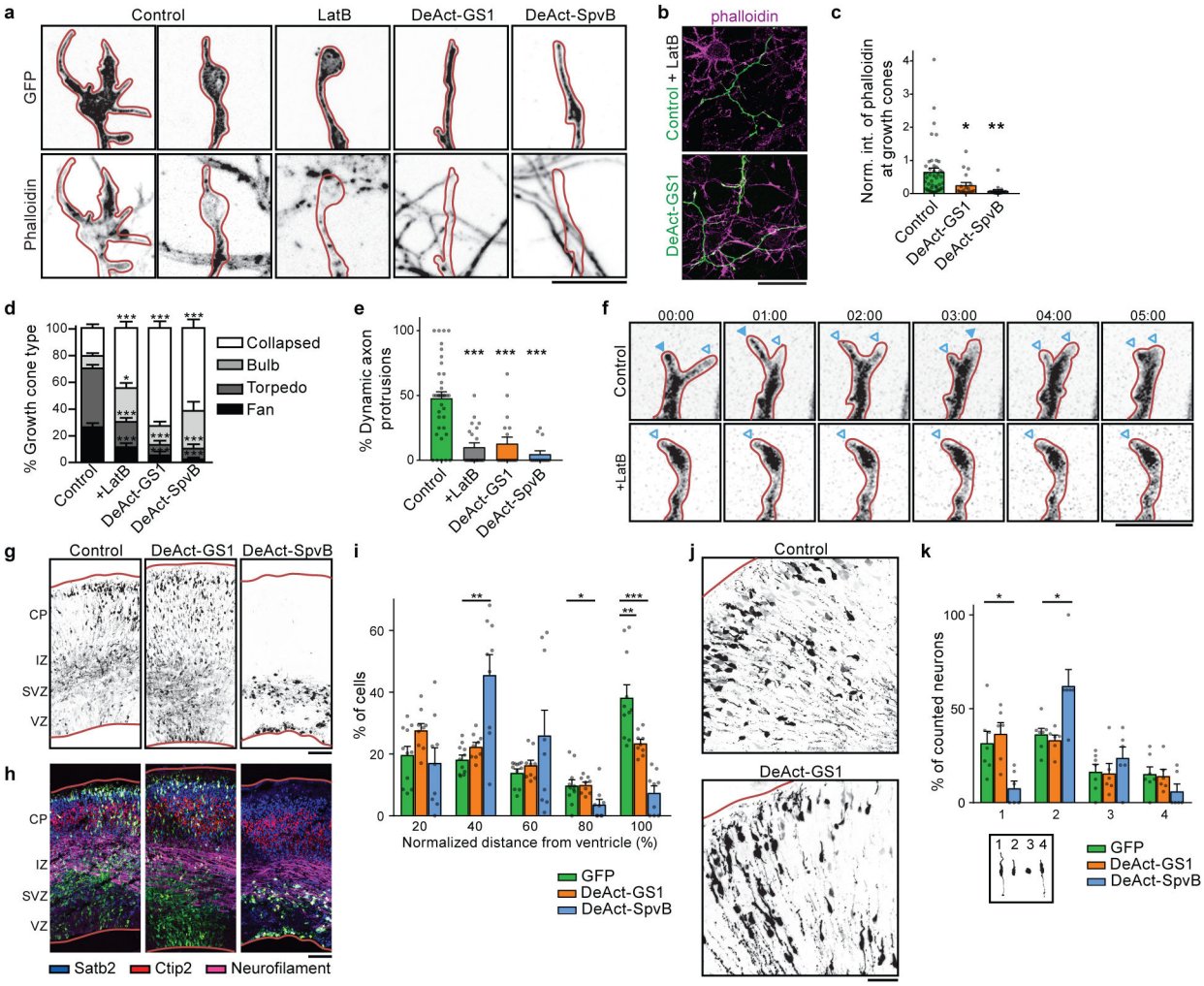

Figure 2. DeActs markedly affect growth cones and neuronal migration

(**a**) Growth cones of DIV4 rat embryonic hippocampal neurons expressing MARCKS-eGFP +/− latrunculin B (LatB) or DeAct-GS1 or DeAct-SpvB and stained with Alexa Fluor 568-phalloidin to visualize actin filaments. Scale, 10 μm.

(**b**) Overview of actin filament staining (magenta) in neuronal cultures expressing MARCKS-eGFP and treated with LatB (affects the whole culture), or expressing DeAct-GS1 (cell-specific). Scale, 40 μm.

(**c**) Quantification of actin filament intensity in growth cones normalized to untransfected neighboring neurons; LatB affects all growth cones, therefore cannot be included (N = 4, 2, 2 independent experiments, n = 44, 19, 22 neurons, left to right).

(**d**) Quantification of growth cone morphology upon MARCKS-eGFP or DeAct expression compared to LatB (N = 4, 2, 2, 2 independent experiments, n = 44, 23, 19, 22 neurons, left to right).

(**e–f**) Dynamics of axonal branches are lost after addition of LatB or in neurons expressing DeAct constructs. A representative example is given in (**f**) from a 5 minute time lapse acquisition. Closed arrow heads indicate growth and open arrow heads represent no growth

or retraction (see also Supplementary Video 3). Scale, 10 μm. (*N* = 4, 2, 2, 2 independent experiments, *n* = 37, 22, 17, 14 neurons, left to right).

(**g–j**) Cortical neuronal migration after *in utero* electroporation with GFP, DeAct-GS1, or DeAct-SpvB. (**g** and **i**) transfected neurons (GFP signal). (**h**) Same slice as (**g**) combined with immunostaining against Satb2 (cortical layer II–IV), Ctip2 (cortical layer IV–V) and Neurofilament (axons in the IZ). CP, Cortical plate; IZ, intermediate zone; SVZ, subventricular zone; VZ, ventricular zone. Scale, **g–h** 100 μm, **j** 50 μm.

(**i**) Quantification of cortical neuronal migration described in (**g**). (*N* = 3 embryos from 3 different litters, *n* = 3412, 2143, 847 cells GFP, DeAct-GS1 or DeAct-SpvB).

(**k**) Quantification of neuronal morphologies of GFP-positive neurons which migrated past the IZ. 1, leading and trailing process; 2, leading process only; 3, no processes; 4, trailing process only (*N* = 3 embryos from 3 different litters, n = 104, 135, 38 cells GFP, DeAct-GS1, or DeAct-SpvB).

Graphs show mean ± SEM. Statistical significance: one-way ANOVA and Dunnett's multiple comparison post hoc test, and Wilcoxon test for paired data, *** $p<0.001$, ** $p<0.01$, * $p<0.05$.

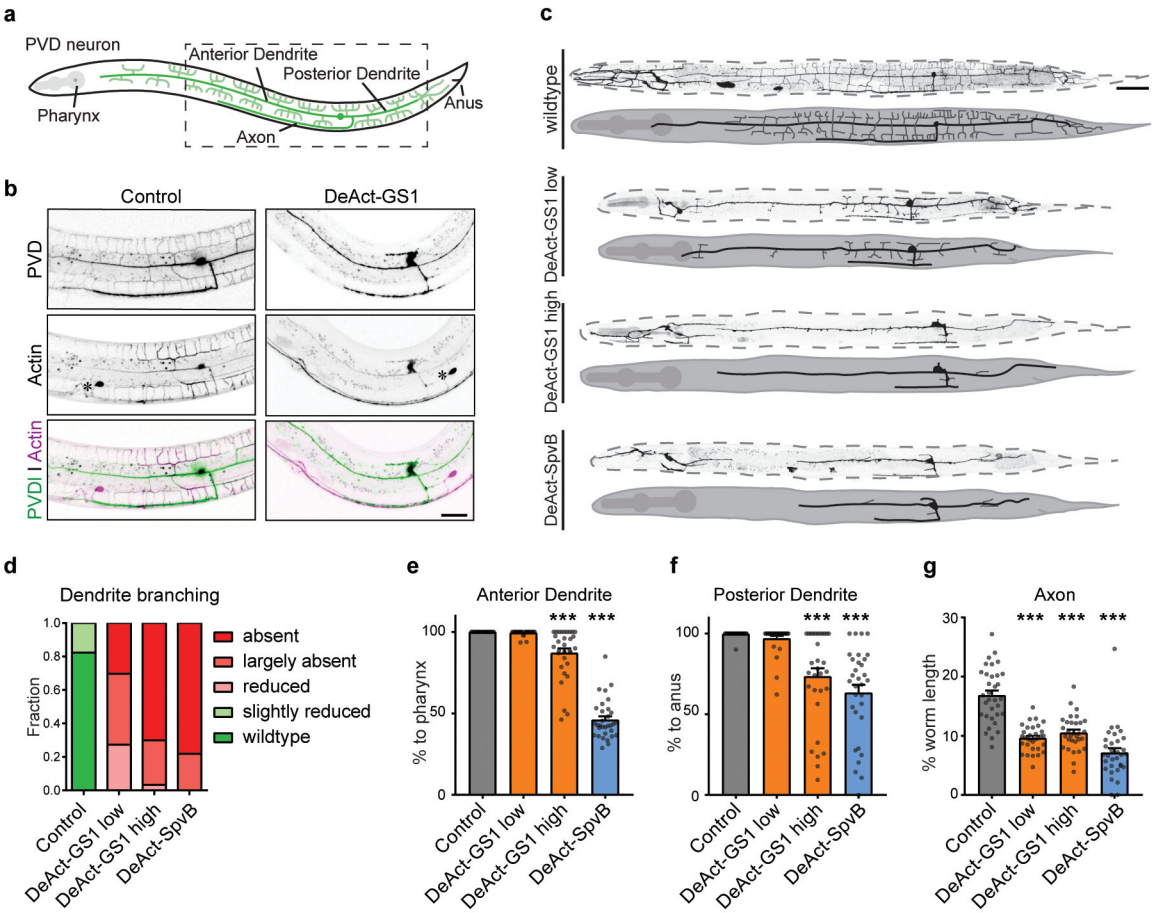

Figure 3. DeActs efficiently inhibit PVD neuron development in C. elegans

(**a**) Schematic representation of the *C. elegans* highly branched PVD neuron.

(**b**) Co-expression of the moesinABD actin marker with GFP (control) or DeAct-GS1 in the PVD neuron. Other neurons expressing the actin marker are marked by *. Scale, 20 μm.

(**c**) Representative images and schematic representation of the PVD neuron morphology upon cell specific DeAct expression. Scale, 50 μm.

(**d–g**) Quantification of the DeAct-induced branching defects (**d**) and primary neurite outgrowth defects (**c–d**). Controls are siblings which lost the DeAct constructs. $N = 34$ for controls and $N = 32$ for DeAct animals (for DeAct-GS1 64 animals were analyzed and split in low and high DeAct expressing animals). Graphs show mean ± SEM. Statistical significance: one-way ANOVA and Dunnett's multiple comparison post hoc test. Micrographs are representative, *** $p<0.001$.